AUTONOMOUS FAULT DETECTION ON A LOW COST GPS-AIDED ATTITUDE DETERMINATION SYSTEM

Arcélio C. Louro, Roberto V. F. Lopes and Hélio K. Kuga

National Institute for Space Research - INPE

Abstract

This paper presents a three-axis attitude determination procedure based on the Global Positioning System (GPS) with special emphasis to the autonomous integrity monitoring issue. One envisages a class of low cost navigation applications requiring low accurate (around 0.5 degrees) but continuous attitude knowledge. A snapshot algorithm first estimate the three-axis attitude from interferometry on double differences of GPS carrier phase L1. Then, the attitude estimate is improved by fusing it with angular rate measurements from low cost, MEMS gyros. The procedure is especially designed to detect single faults on either the GPS or the gyros autonomously from residuals monitoring. Both GPS and gyro measurements are taken as corrupted by colored Gaussian noises whose effects are mitigated by a stochastic dynamic compensation model. The state vector, which includes the attitude quaternion and parameters of the error model, is estimated from a bank of extended Kalman filters with different time delays. Attitude propagation model between GPS sampling times is based on the gyro output after drift calibration. One defines the fault modes of each sensor and some control parameters to the fault detection procedure.The algorithm is tested with numerical simulation and real data. The simulation scenarios include LEO micro-satellites with different orbit inclinations and three different failure modes: complete out track from the whole GPS constellation; temporary abnormal interference on a single GPS satellite; and gyro drift higher than its specified level. The results show that the algorithm is suitable to cope with different fault types and intensity levels.

1. INTRODUCTION

This work presents an algorithm for three-axis autonomous attitude determination, envisaging future applications mainly in micro-satellites. The algorithm is based on inertial sensors using MEMS (Micro Electro-Mechanical Systems) technology aided by GPS (Global Positioning System) and is able to keep working under temporary single faults either in the gyros or in the GPS. Specifically, we use a set of three-axis silicon Vibrating Ring Gyros based on the Coriolis Effect that presents a promising long term stability [1] compatible with a class of space missions with moderate pointing requirements and stringent budgets in terms of cost, weight, volume and power consumption. However, the algorithm is not constrained to space applications of any special type.

The gyro drift is compensated by interferometry on double differences of GPS carrier phase L1 as observed by a set of at least three GPS receivers, each one with single antenna inputs. The robustness required for autonomous space applications, is ensured by fault detection and diagnosis techniques basically relying in the GPS redundant information.

As discussed in Reference [2], we concentrate in three Gyro and GPS fault modes: GPS signal contingency outages; GPS signal under unexpectedly strong interference; and gyros with long term drift higher than the specified limits. Fault detection nomenclature follows Reference [3] (see also [2]). The algorithm is adapted from the work of McMillan, Bird and Arden [4]. Under a temporary interruption of GPS signal lock, attitude is propagated from gyros alone. High interference on a signal from one GPS receiver is detected and solved by checking the residuals of the remaining healthy ones. High gyro noise level is detected and isolated by a bank of attitude propagators with different time delays in a Kalman filter schema.

This work was developed in the frame of the doctoral thesis of the first author at INPE [5]. Partial results with focus on the GPS solution were presented in Reference [2]. Preliminary results of the GPS and gyro data fusing were also presented in Reference [6] showing simulation results with a single attitude propagation delay to detect Gyro faults. In this work we present the algorithm on its plain capacity, with real GPS experimental data and simulation of multiple delays in the Gyro fault detection part of the algorithm.

Other important issues for autonomous implementation of GPS based attitude determination like integer ambiguity resolution, on board multipath mitigation and antenna phase center calibration have been addressed by the second author and his collaborators [7-10] and are not the aim of the present work.

2. Gyro and GPS Integration

When integrated with Gyros, a GPS receiver provides means to calibrate the long term gyro drift, and consequently allows precise attitude propagation with a sample rate higher than the GPS receiver usually operates. Moreover, the attitude propagated by Gyros provides important information during GPS loss of signal. In addition, in the absence of faults, the attitude is estimated with better accuracy than the GPS-based only solution. This makes the approach particularly suitable for real time spaceborn application, including closed loop attitude control. That is why it is so important to detect, insolate and as much as possible to correct any fault in the system autonomously.

The integration between GPS receiver and Gyro can be made by structures with different degrees of coupling [11]. In this work we follow the loosely coupled solution, with direct feedback structure that is suitable for use of independent, off the shelf equipment.

The algorithm is divided in two steps. First, attitude is determined by a snapshot algorithm from the GPS data. Then, the gyro data is added and the attitude is estimated together with other system parameters by the Kalman filter, as described in the sequence.

2.1. Static Attitude Determination

The GPS attitude determination used here follows directly from Reference [12] for 3-axis attitude determination using three or more GPS antennas.

The algorithm uses double differences of carrier phase:

$$\varphi_{i,0}^{p,0} = \frac{1}{\lambda}(s^{p,0})' b_{i,0} + N_{i,0}^{p,0} + d_{i,0}^{p,0} + \varepsilon_{i,0}^{p,0} \tag{1}$$

where $\varphi_{i,0}^{p,0}$ is the double difference between antenna i to the master antenna 0 and between GPS satellites p to a reference satellite 0; λ is the L1 wavelength; s is the GPS satellite line of sight; N is the integer ambiguity; d is the delay due to multipath among other factors and ε is a random noise.

First the GPS data is pre-processed to deal with integer ambiguity and antenna calibration. After that, a static (snapshot) attitude determination is carried out, that minimizes the following quadratic cost function, which takes in to account the intrinsic coupling due to the presence of master antenna and reference GPS satellite in every double difference:

$$J = tr\left\{\left[Y - \frac{1}{\lambda}B'AS\Delta_m{}'\right]\Lambda_m\left[Y - \frac{1}{\lambda}B'AS\Delta_m{}'\right]'\Lambda_n\right\} \tag{2}$$

where Y is the matrix of double differences of carrier phase after integer ambiguity resolution, $tr\{\}$ is the matrix trace operator, B is the antenna baseline matrix in the body frame, A is the attitude matrix, S is the matrix of line of sights of locked GPS satellites in the reference frame, Δ_m is the matrix operator responsible to implement between satellite differences and Λ_n and Λ_m are the decoupling matrices defined in Reference [12].

Excluding faults, the minimum value of the cost function J should present a Chi-square distribution with $\mu = (n-1)(m-1)-3$ degrees of freedom, where m is the number of satellites and n is the number of GPS antennas. This property will be useful to detect faults on GPS signals in next session.

2.2. Attitude Filtering

For the attitude filtering and propagation the algorithm is based on Reference [13] that applies the Kalman filter to three-axis attitude estimation based on the cinematic model In our case, the Gyro is a simple MEMS device and the attitude sensor is a GPS receiver, whose attitude snapshot solution works as a quaternion sensor.

The rate of change of the attitude matrix with time is driven by the angular velocity vector ω in the satellite system, and may be represented in quaternion algebra by:

$$\dot{\bar{q}}(t) = \tfrac{1}{2}\Omega(\omega(t))\bar{q}(t) \tag{3}$$

where the unit quaternion $\bar{q}$ is composed of a vector q and a scalar q_4 :

$$\bar{q} = \begin{bmatrix} q \\ q_4 \end{bmatrix} \tag{4}$$

Matrix $\Omega(\omega(t))$ is defined below:

$$\Omega(\omega) = \begin{bmatrix} 0 & \omega_3 & -\omega_2 & \omega_1 \\ -\omega_3 & 0 & \omega_1 & \omega_2 \\ \omega_2 & -\omega_1 & 0 & \omega_3 \\ -\omega_1 & -\omega_2 & -\omega_3 & 0 \end{bmatrix} \tag{5}$$

The attitude propagation model is given by a simple cinematic model given by Equation 3, and a gyro model disturbed by a first order Gauss-Markov stochastic process which represents the Gyro long term drift-rate bias, and a white noise. Similarly, the GPS-based attitude is modeled as an attitude observation corrupted by a white noise stochastic sequence and a first order Gauss-Markov stochastic process that takes into account the time correlation observed in the GPS phase signal. So, the dynamic model is given by the following equations:

$$u = \omega + \beta_\omega + e_\omega(C_{\omega\omega}) \tag{6}$$

$$\dot{\beta}_\omega = -\frac{\beta_\omega}{\tau_\omega} + w_\omega(q_\omega) \tag{7}$$

$$Z = \theta + \beta_\theta + e_\theta(C_{\theta\theta}) \tag{8}$$

$$\dot{\beta}_\theta = -\frac{\beta_\theta}{\tau_\theta} + w_\theta(q_\theta) \tag{9}$$

where *Z* is the input vector observation to the Kalman filter, coming from the GPS, β_ω is the long term gyro drift, β_θ is a time correlated noise in the GPS-based attitude estimate. The model parameters q_θ, q_ω and τ_θ, τ_ω represents respectively the noise intensity and time constants of the correlated bias β_θ and β_ω; e_ω is the gyro noise, $C_{\omega\omega}$ is its covariance matrix, e_θ represents the GPS-based attitude noise and $C_{\theta\theta}$ its covariance matrix.

All those model parameters were fitted empirically from experimental data (see [12]).

The well-known singularity on quaternion covariance matrix is managed following the reduced covariance approach presented by [13]. Then, the reduced state vector that will be actually estimated is:

$$\underline{x}(t) = \begin{bmatrix} \Delta\underline{q}(t) \\ \beta_\omega \\ \beta_\theta \end{bmatrix} \tag{10}$$

where $\Delta\underline{q}$ is the reduced quaternion increment from the GPS-based attitude to the attitude propagated by the Gyro (from Eq. 9) and the quaternion propagated by the Gyro.

3. Fault Diagnosis

A fault is a deviation not permitted of at least one characteristic property or variable of the system from acceptable, usual or standard behavior [3], in contrast to a failure, which is considered a permanent interruption of the system ability to perform any required function under specified operating conditions. Fault detection is here understood as the determination that the system presents a fault; fault isolation determines the kind and location of a fault; and fault identification determines the fault intensity. Fault diagnosis deals with fault detection, isolation and identification. The proposed procedure envisages single fault diagnosis only, either on the GPS or on the gyro. Permanent failures or multiple faults are not considered.

A fault occurrence has degradation consequences in the level of uncertainty of the estimated attitude. The level of degradation depends on the fault and from the algorithm success to detect faults, established by the percentage of false alarms and by the percentage of faults not detected. In case of temporary fault detected in the Gyro signal, the level of uncertainty growth, but only until the level obtained by the solution using GPS alone. The occurrence of a fault in the GPS signal can induce partial or complete degradation in the uncertainty level, depending on the fault duration and intensity.

Considering a mask angle of 10°, the number of GPS constellation satellites in view from an Earth pointing satellite in Low Earth Orbit ranges from 6 to 8 most of the time. This number may even increase significantly with the advent of other GNSS constellations. In this scenario, there is internal sufficient redundancy to detect fault on the GPS during the phase of static attitude determination. This detection is made by a group of parallel processors where in each processor one of the GPS satellites is suppressed, as indicated in part b of diagram shown in Fig. 1.

The second part of the proposed algorithm uses a Kalman filter to update the quaternion, the Gyro drift-rate bias and the GPS error corrections. After the state update step, the attitude is propagated using the drift-compensated Gyro output, with a sample frequency higher than the attitude obtained from GPS alone.

In case of a single fault either on GPS or Gyro, the attitude solution continuity is assured by the remaining wealthy sensor, which allows a complete fault diagnosis.

The fault diagnosis algorithm have some control parameters that need to be tuned empirically. The efficiency of the algorithm follows directly from this adjustment. More specifically, they determine the false alarm rate and the missing fault detection rate.

3.1. GPS Fault Diagnosis

Part b of Fig. 1 shows the parallel processors that implement the GPS fault diagnosis Box which makes the comparison of all the cost functions and send to the Kalman filter the fixed estimate of attitude matrix and its error covariance matrix.

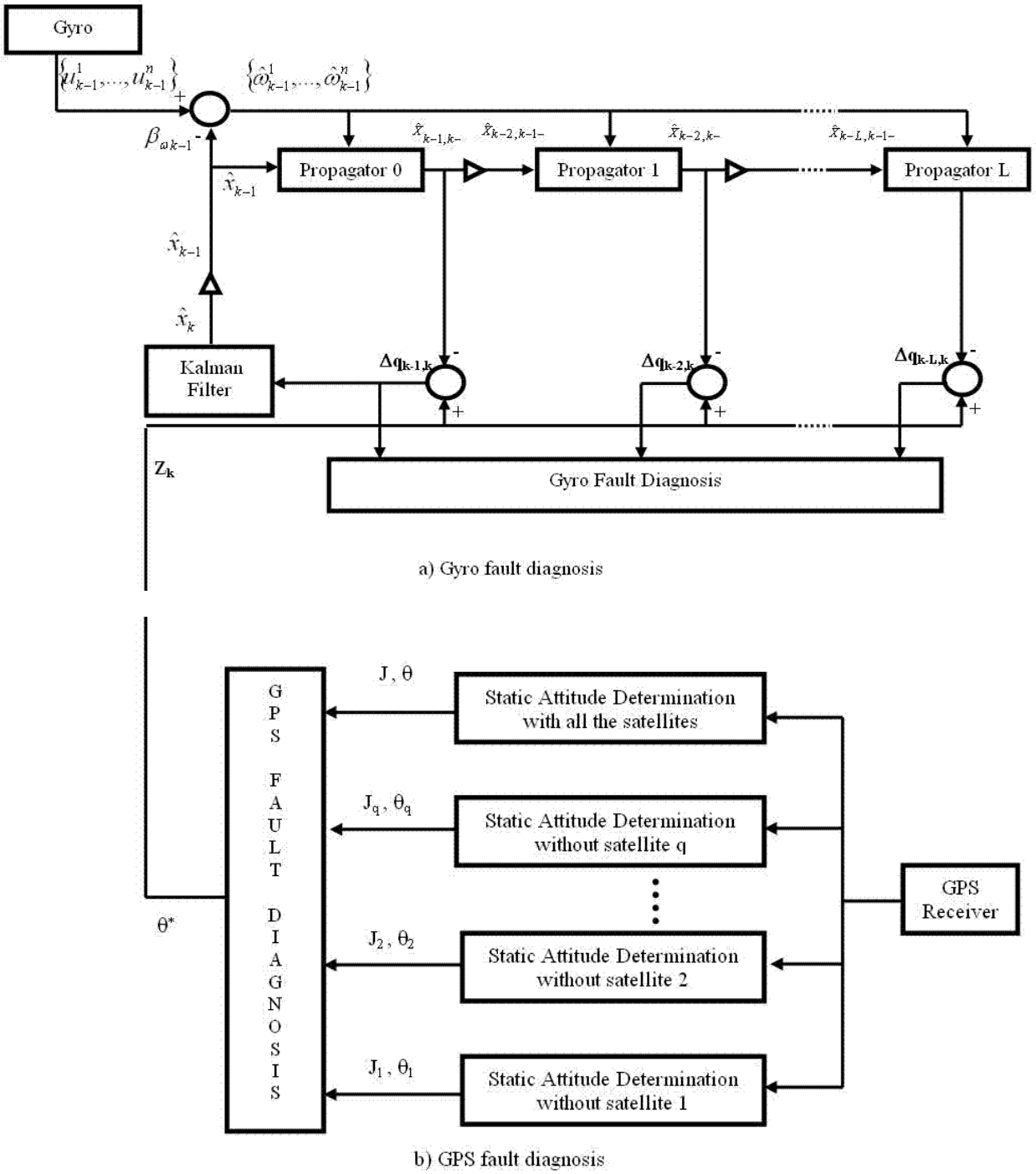

Figure 1. Fault diagnosis algorithm schema.

If $J_p < J_\bullet \ \forall p$, where p is the number of the processor that excludes data coming from p-th GPS satellite, and $J_\bullet$ is the fault detection threshold, the algorithm considers that there is no detectable fault and takes $\theta^* = \theta$. Otherwise, if $J_p > J_\bullet \ \forall p \neq q$, but $J_q < J_\bullet$, then a fault is detected in satellite q, and one takes $\theta^* = \theta_q$. There are *m* processors: one to the full constellation and *m*-1 to isolate possible faults. If $J_p > J_\bullet \ \forall p$, it is necessary to repeat the test with a different reference satellite because it may be the faulty one.

Since in absence of faults J has chi-square distribution with μ degrees of freedom, it is convenient to express the threshold $J_\bullet$ as $\mu_J + \kappa\sigma_J$, where $\sigma_J = \sqrt{2\mu_J}$ is the standard deviation of J and κ is the control parameter that should be somewhere in the practical range from 0 to 5 and was set to 3 from simulation analysis.

3.2. Gyro Fault Diagnosis

Part a of Fig. 1 shows the Kalman filter fed by information from the difference between the Gyro propagated quaternion and the estimated attitude coming from the GPS. The Filter equations are standard and follow directly from Reference [13] with a minor variation due to the additional state variable β_θ which has a very simple dynamics and is not coupled with the other state variables. Therefore we may concentrate in the quaternion propagation equation. If the rotation vector defined as:

$$\Delta\theta = \int_t^{t+\Delta t} \omega(t')dt' \tag{12}$$

is small, then the solution of Eq. 3 is given by:

$$\bar{q}(t+\Delta t) = M(\Delta\theta)\bar{q}(t) \tag{13}$$

where

$$M(\Delta\theta) = \cos(|\Delta\theta|/2)I_{4x4} + \frac{sen(|\Delta\theta|/2)}{|\Delta\theta|}\Omega(\Delta\theta) \tag{14}$$

Gyro is considered faulty if the residues of Equation 8 grow above a tolerance level proportional to its theoretical standard deviation. This is illustrated in next section, with some numerical results.

4. Simulation and Experimental Results

Reference [2] shows simulation results of the GPS part of the algorithm (part b of Fig. 1). Rference [6] shows simulation results of the GPS and Gyro parts considering only one delay in the gyro part of the algorithm (part a of Fig. 1). This work completes those previous works with an arbitrary number of time delays and present experimental results of the GPS part taken on ground, in connection with simulated Gyro data. Also, we present more extensive simulation results with two different orbit scenarios.

Faults on the GPS signals may occur for instance due to receiver electronics instability and environment interferences, including multipath. In order to test the procedure, single faults were simulated on the GPS signals. These faults are not associated with any specific physical event, but they intend to demonstrate the sensitivity of the fault diagnosis procedure to the intensity of an arbitrary fault.

The simulation considers a square structure with lateral of 1 meter where three GPS antennas are positioned and the Gyro are simulated perfectly aligned with this structure to sense the same movement in three axes. Antenna number 0 is positioned at the corner of a square and was taken as the master antenna. Antenna number is 2 positioned in the x direction with respect to the master antenna and antenna number 1 in the y direction, forming two orthogonal baselines, namely baseline 0-2 and baseline 0-1.

4.1. GPS Experimental Data

The Experimental data taken was carried out using three commercial GPS receivers with a sample rate of 1Hz. An intentional fault injection was performed by adding 5 cycles between instants 30s and 40s in GPS satellite 27 that simulates an error in the integer ambiguity resolution algorithm in order to illustrate the fault detection performance.

As shown in Figure 2, during the introduction of the failure the cost function for all data combination increased dramatically but for the faulty satellite p = 27. Figure 3 presents the 3-axis attitude estimated from GPS only, after fault detection. Those values feed the Kalman filter as input measurements and do not present any visible degradation due to the fault. More details may be found in [5].

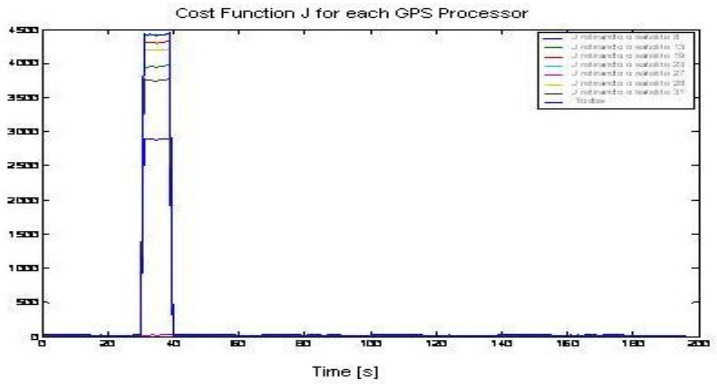

Figure 2. Cost function.

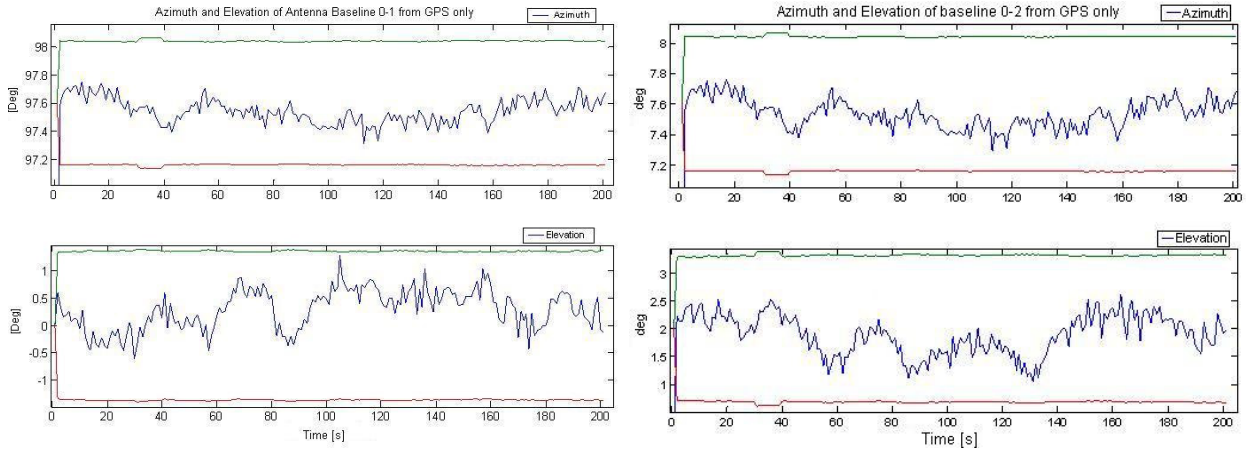

Figure 3. Three-axis attitude estimates from GPS only, and respective 1 sigma uncertainty boundaries.

4.2. Gyro Data Simulation

A MEMS Gyro with the characteristics described in Reference [14] (See also [15]) was simulated using commercial software Spacecraft Control Matlab Toolbox from Princeton Satellite Systems. Two different simulations are presented here to explore different aspects, as described in the sequence.

4.2.1. Gyro - First Case: effect of number of time delays in the bank of attitude propagators

In this case, intentional fault injection was performed by introducing an error of 0.03 rad/s in the drift-rate bias during the interval from 70s to 80s. The gyro fault detection was performed using two delayed propagators. Figure 4 shows both filtered and propagated 3-axis attitude by the propagator with two time delays, while Figure 5 shows the estimates of quaternion increment (Δq) by both filter-propagator processes. In Figures 4 and 5, the filtered 3-axis attitude is shown with the GPS sampling rate of 1 Hz, while gyro propagated attitude is shown with a higher sampling rate of 10Hz.

The algorithm was able to detect the gyro fault between instants 70s to 80s since q_2 clearly exceeded its 1-sigma uncertainty level in both propagators. However, the effect was much stronger in the propagator with the longest delay.

As a marginal general observation that may be useful in some applications, one can see from Figures 3 to 5 that azimuth estimates are more accurate than elevation estimates. This fact is confirmed by simulations and may be related with the special distribution of GPS constellation.

4.2.2. Gyro - Second Case: effect of GPS signal outage

Figure 6 shows the quaternion increment (Δq) considering complete loss of the GPS signal in the interval from 70s to 100s. In this case, the gyro propagates the attitude not considering the GPS. As a consequence, the error level increases fast during this interval but quickly recover its normal accuracy level after the instrument recovers itself from the faulty condition.

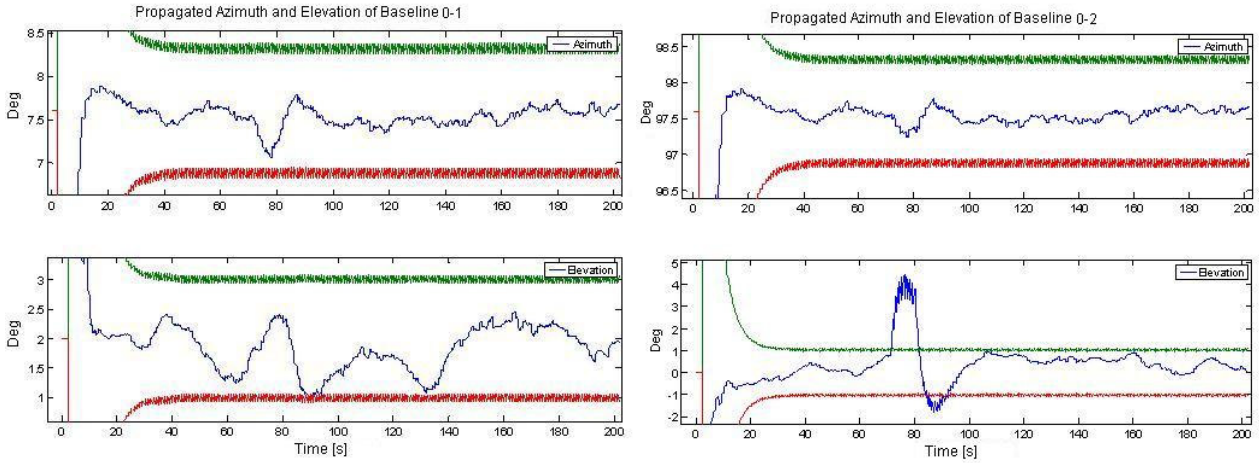

Figure 4. Three-axis filtered and propagated attitude (Attitude matrix converted to azimuth and elevation) and respective 1 sigma uncertainty boundaries: a) Antenna baseline 0-1; b) Antenna baseline 0-2.

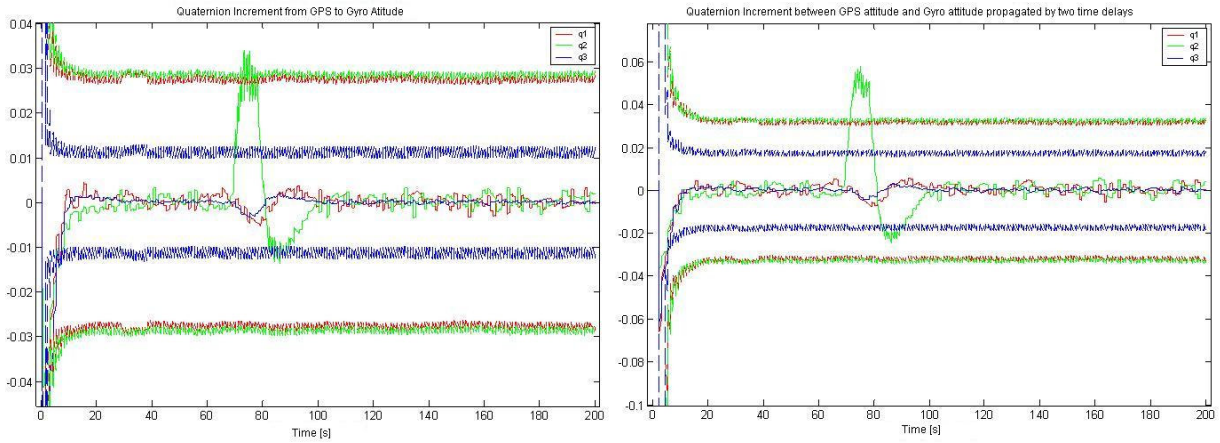

Figure 5. State Estimates and their 1-sigma uncertainty boundaries: a) attitude propagation with a single time delay; b) attitude propagation with two time delays.

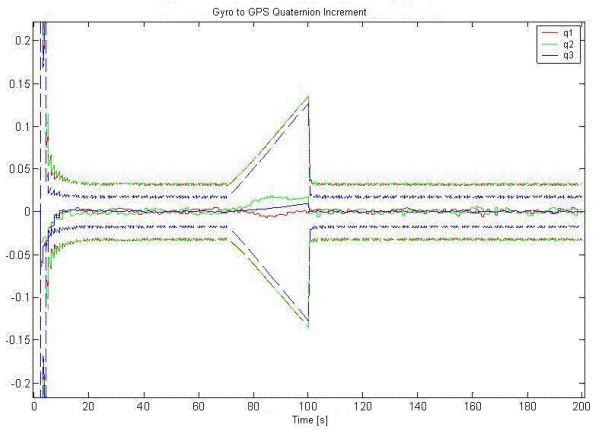

Figure 6. Quaternion increment between GPS and Gyro attitudes, and respective 1 sigma boundaries.

4.3. Flight Conditions Simulation

In addition to the experiments briefly described in the previous sessions, simulations were performed to test the algorithm in orbit conditions. Two orbit scenarios are selected with this purpose: one circular polar orbit and one circular, low inclined orbit. In both cases the orbit altitude is set to 650 km and the satellite is in Earth-oriented three-axis stabilization with residual oscillations caused by attitude control errors (pointing accuracy better than 1^{o} and drift

rate below 0.1°/s). The simulations run for one orbit period to check the influence of different relative geometry of line of sight to the GPS satellites. Other simulation parameters are given in Table 1. Besides addition of noise, the L1 phase is affected by multipath delays with medium level correspondent to 50% of the strong multipath scenario caused by a pair of metal plates in the close neighborhood of the antennas, as described in [10]. Gyro fault injection happens in a ten minutes extra time after end of the one orbit simulation, which is time enough to the algorithm to detect it.

Table 1 – Attitude Sensor Parameters in the Simulation

Long term Gyro stability:	48μ-rad/s (10°/h)
Gyro Random walk:	20 μ-rad/√s (0.066°/√h)
Gyro sampling rate:	10 Hz
GPS sampling rate:	0.2 Hz
Antenna baseline:	0.6 m
L1 Phase Uncertainty (before double difference):	1% of L1 wavelength
GPS mask angle:	15°
Mean time between fault injection on GPS:	60 s
intensity of GPS fault injection:	35% of L1 wavelength
Intensity of gyro fault injection	10 times the gyro drift

Intentionally, the integer ambiguity is solved every sample time in order to check the performance of this part of the algorithm under different orbit and attitude conditions.

Several tests were run in order to check the effect of control parameters of the fault diagnosis algorithm as well as to explore the effect of error levels in both attitude sensors. Typical results from the Equatorial orbit scenario are summarized in Table 2. No special difference was found in the polar orbit scenario. Figures 7 and 8 show the attitude errors and their statistics. The advantage of data fusion in terms of accuracy is clear in all axes. Furthermore, the problem of worse accuracy given by the GPS alone around pitch and roll-axes is minimized. Also, as the GPS is more accurate around yaw axis, it clearly improves the accuracy of the Kalman filter estimate when compared with the gyro propagated solution in a profitable cooperation between these sensors.

The results give evidence on the advantage of having more than one time delay in the Gyro fault detection algorithm. After 5 time delays, the gain in the fault detection was marginal.

Table 2 – Summary of Simulation Results

Failure rate on Integer Ambiguity Solution:	0 %
Rate of GPS Missed Faults:	2 %
Rate of GPS False Alarms:	40%
Time delay to detect gyro fault by 1st propagator:	450s
2nd propagator:	220s
3rd propagator:	190s
4th propagator:	190s
5th propagator:	125s
Rate of Gyro False Alarms:	0%

Conclusions

An attitude determination algorithm is presented based on MEMS gyros aided by GPS. Tested under different flight simulated conditions as well as with ground taken real data, the algorithm presented robustness to the following fault modes of the attitude sensors: GPS temporary loss of signal; high interference on GPS carrier phase signal; and unpredicted high level of gyro drift.

This algorithm explores the benefits of both sensors with different characteristics that may be attractive to low cost micro-satellites. The algorithm is potentially promising specially considering that the number of GNSS systems is foreseen to increase in the near term and the stability of MEMS gyros are improving systematically with time and may become a key instrument to cheap attitude determination systems. In this context, the paper intends to give a contribution to make it a reality.

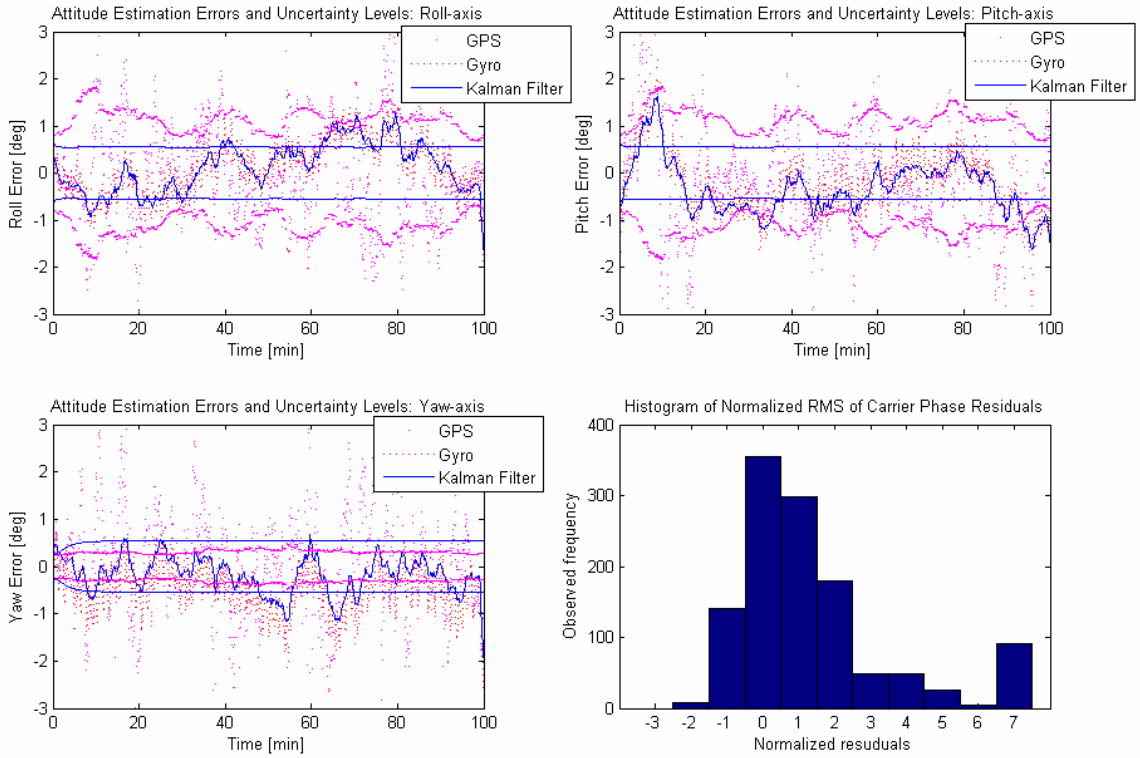

Figure 7 – Attitude errors in Roll, Pitch and Yaw axes from GPS, gyro and Kalman filter, and histogram of normalized residuals of GPS carrier phase.

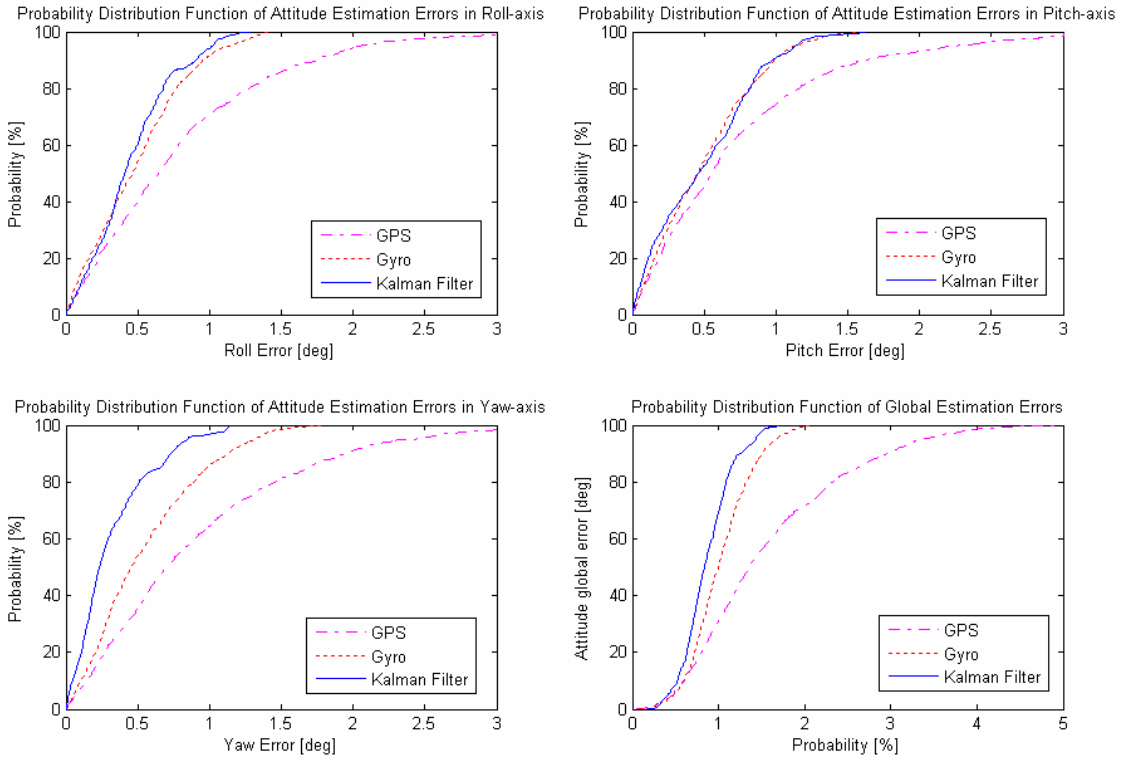

Figure 8 – Observed Probability Distribution Function of attitude errors in Roll, Pitch and Yaw axes and global attitude error from GPS, gyro and Kalman filter.

References

1. El-Sheimy, N and Niu, X. "The Promise of MEMS to the Navigation Community." Inside GNSS, pp. 46-56. Mar-Apr, 2007.

2. Louro, A.C. and Lopes, R.V.F. "Diagnose de Falhas na Determinação Autônoma de Atitude de Micro-Satélites por meio de GPS e Giros". *IV Simpósio Brasileiro de Engenharia Inercial – SBEIN*, São José dos Campos, Brazil, Nov. 2004.

3. Nyberg, M. *Model Based Fault Diagnosis Methods, Theory, and Automotive Engine Applications*. Department of Electrical Engineering, Linköping University, Linköping, Sweden, 1999. [Dissertation No. 591].

4. McMillan, J. C.; Bird, J. S. and Arden, D. A. G. "Techniques for Soft-Failure Detection in a Multisensor Integrated System." *Journal of The Institute of Navigation*, Vol. 40, No. 3, Fall 1993, pp. 359-380.

5. Louro, A.C. *Autonomous Spacecraft Attitude Determination Using GPS*. INPE, São José dos Campos, Brazil, 2006. (Doctoral thesis, in Portuguese). [INPE-14091-TDI/1074]

6. Louro, A.C., Lopes, R.V.F. "Fault Diagnose In The Autonomy Micro-Satellite Attitude Determination Using GPS And Gyros: Simulation Results". *18th International Congress of Mechanical Engineering – COBEM 2005*. Ouro Preto, Brazil, Nov. 6-11, 2005.

7. Lopes, R. V. F, Carrara, V., Enderle, W. "Multipath Mitigation by Neural Network for Spacecraft Attitude Determination from GPS Carrier Phase Observables."*10th Australian International Aerospace Congres. Proceedings,* Mee, D. J. (Ed), paper 091. Brisbane, 29 July – 1st Aug., 2003. [ISBN 085-825-733-5].

8. Lopes, R. V. F. "Integer Ambiguity Resolution for Spacecraft Attitude Determination Using GPS." *Proceedings of ION GPS 2002*, pp. 1088-1093. Portland, OR, USA, 24-27 Sept., 2002.

9. Lopes, R. V. F. and Milani, P. G. "Consistent On-Board Multipath Calibration for GPS Based Spacecraft Attitude Determination." *Proceedings of ION GPS 2000*, pp. 2216-2226. Salt Lake City, USA, 19-22 Sept., 2000.

10. Lopes, R. V. F.; Carrara, V.; Enderle, W. and Arbinger, C. "Mitigating Multipath by Neural Network." (AAS 00-207) Advances in the Astronautical Sciences, Vol. 105, Part II, pp. 1639-1650, 2000.

11. Kaplan, E. D. *Understanding GPS: principles and applications*, London, UK.1996.

12. Lopes, R. V. F.; Silva, A. R.; and Prado, A. F. B. A. "Navigation and Attitude Estimation from GPS Pseudorange, Carrier Phase and Doppler Observables." 53rd *International Astronautical Congress IAC*, Houston, Texas, USA, Oct. 10-19, 2002.

13. Lefferts, E.J., Markley, F.L. e Shuster, M.D. "Kalman Filtering for Spacecraft Attitude Estimation". *Journal of Guidance, Control, and Dynamics*, Vol. 5, pp. 417-429. 1982.

14. Crista. "Crista IMU Specification." 2005 http://www.cloudcaptech.com/crista_imu.htm.

15. Brown, A.K. and Lu, Y. "Performance Test Results of an Integrated GPS/MEMS Inertial Navigation Package". ION GNSS 2004, Long Beach, CA, Sep. 2004.